Molecular Therapy
Oncolytics
Original Article

Characterization and quantitation of busulfan DNA adducts in the blood of patients receiving busulfan therapy

Valeria Guidolin,[1,3,5] Yupeng Li,[1,2,5] Foster C. Jacobs,[1,3] Margaret L. MacMillan,[1,4] Peter W. Villalta,[1,2] Stephen S. Hecht,[1] and Silvia Balbo[1,3]

[1]Masonic Cancer Center, University of Minnesota, Minneapolis, MN 55455, USA; [2]Department of Medicinal Chemistry, University of Minnesota, Minneapolis, MN 55455, USA; [3]School of Public Health, University of Minnesota, Minneapolis, MN 55455, USA; [4]Blood and Marrow Transplantation & Cellular Therapy Program, Department of Pediatrics, University of Minnesota, Minneapolis, MN 55455, USA

DNA alkylating drugs have been used as cancer chemotherapy with variable outcomes. The establishment of predictive biomarkers to identify patients who will effectively respond to treatment would allow for the development of personalized therapies. As the degree of interaction of alkylating drug with DNA plays a key role in their mechanism of action, our hypothesis is that the measurement of the DNA adducts formed by alkylating drugs could be used to inform patient stratification. Beginning with busulfan, we took advantage of our DNA adductomic approach to characterize DNA adducts formed by reacting busulfan with calf-thymus DNA. Samples collected from six patients undergoing busulfan-based chemotherapy prior to allogeneic hematopoietic cell transplantation were analyzed for the presence of busulfan-derived DNA adducts. Among the 15 adducts detected *in vitro*, 12 were observed in the patient blood confirming the presence of a large profile of DNA adducts *in vivo*. Two of the detected adducts were structurally confirmed by comparison with synthetic standards and quantified in patients. These data confirm our ability to comprehensively characterize busulfan-derived DNA damage and set the stage for the development of methods to support personalized chemotherapy.

INTRODUCTION

Alkylating drug-based chemotherapy remains the first-line treatment choice for many types of cancer dating back to when nitrogen mustard was first introduced in 1940s.[1,2] To achieve their therapeutic effect, alkylating drugs must enter cancer cells and dysregulate cell cycles by modifying the DNA structure.[3,4] DNA damage is the desired effect on cancer cells as it leads to cell replication blockage and subsequent cell death, but it is also the cause of side effects when localized in healthy cells. Large variations in efficacy and toxicity of alkylating drugs have been widely observed in the clinic. Since an association between alkylating drug-based chemotherapy outcome and cancer cell DNA modifications has been established, it is reasonable to investigate the use of DNA damage products formed by alkylating drugs for patient stratification.[5] Due to the development of new analytical technologies, it is now possible to characterize DNA damage and quantify the levels of specific types of DNA damage products. For example, in the blood DNA of patients receiving platinum drugs, the levels of DNA platinum adducts were shown to be closely associated with therapy outcome.[5–8] To better understand the profile of DNA damage caused by alkylating drugs, we have developed a DNA adductomic method that allows us to comprehensively study the DNA adduct formation by using high-resolution mass spectrometry (HRMS).[9] On the basis of this method, we report here the first study of DNA adduct formation caused by the widely used frontline alkylating drug busulfan (BU) (1,4-butanediol dimethanesulfonate, **1**; Figure 1).

BU is an alkylating agent historically used for the treatment of a variety of cancers.[10] BU is nowadays frequently used in combination with other chemotherapeutic agents for pre-transplantation conditioning of patients undergoing allogeneic hematopoietic cell transplantation (HCT).[11,12] Similar to other alkylating drugs, BU-based therapy side effects include bone marrow suppression, myelosuppression, and hyperpigmentation.[10] Although a clear benefit has been observed using a regimen of cyclophosphamide (CY) with high-dose oral BU in pre-transplantation conditioning,[13,14] high systemic exposure to BU has been associated with neurotoxicity and other conditions.[15–17] Low systemic exposure to BU, however, may result in leukemic relapse and increased risks of graft rejection.[18,19] Altogether, these observations indicate a narrow therapeutic window for BU-based therapy in the clinic.[20]

To inform the optimal dose of BU for cancer patients, efforts have been made to monitor its concentration in plasma.[21–23] However, controversies regarding the advantage of monitoring systematic exposure of BU have been reported due to the presence of

Received 14 June 2022; accepted 18 January 2023;
https://doi.org/10.1016/j.omto.2023.01.005.

[5]These authors contributed equally

Correspondence: Silvia Balbo, Masonic Cancer Center, University of Minnesota, 2231 6th Street SE - 2-145 CCRB, Minneapolis, MN 55455, USA.
E-mail: balbo006@umn.edu

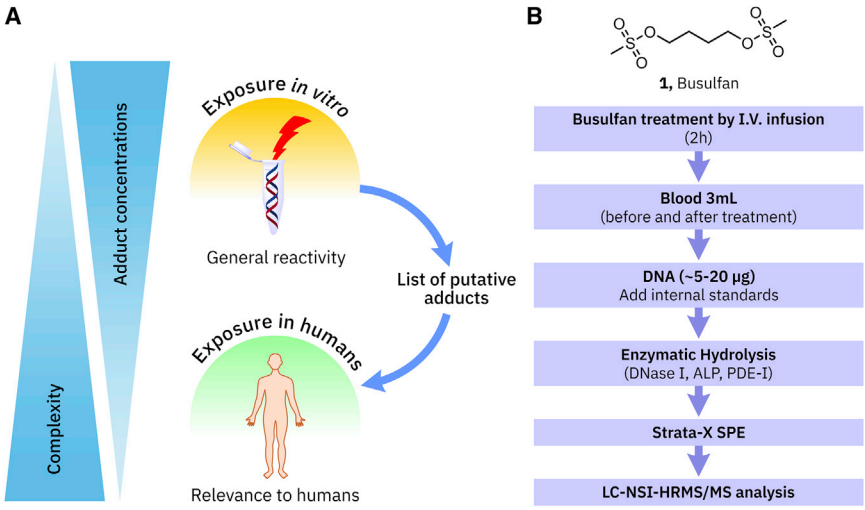

Figure 1. Study rationale and sample workflow

The study rationale (A) and the work flow (B) of adductomic analysis of DNA samples. In the *in vitro* conditions with less complexity, DNA adducts are more readily identified due to their higher concentrations. This allows for a DNA adduct library generation that can be informative for *in vivo* evaluation of patient DNA samples.

confounders.[20] Indeed, many retrospective studies evaluating the association of BU exposure to clinical outcomes were confounded by heterogeneity in the conditioning regimens and the baseline patient characteristics.[20]

In this context, BU-derived DNA adducts can be considered as clinical outcome prediction biomarkers since they are the direct products resulting from BU therapy. The evaluation of their profile could provide more accurate information on the interaction of the drug with its target to be used to support predictive information for adjusting BU dose. This may be even more important when BU is used in combination with other alkylating drugs due to the observed BU-related drug-drug interactions.[24] However, to the best of our knowledge, these DNA adducts were only hypothesized to take part in BU-related cytotoxicity and had not been fully characterized before.[25] Using our above-mentioned adductomic approach,[26–28] we report here the first comprehensive study of BU-DNA adducts formed *in vitro* in BU-treated calf-thymus and bacterial DNA, along with the synthesis and characterization of two of the major identified BU-DNA adducts. Detection of the adducts *in vivo* in the blood DNA of cancer and Fanconi anemia patients receiving BU therapy was demonstrated, along with the establishment of a quantitative method for use in large sample population studies.

RESULTS

Analysis of putative BU DNA adducts formed *in vitro*

A top-down DNA adductomic approach was utilized for the comprehensive characterization of BU-derived DNA adducts in calf-thymus DNA(CT-DNA), treated with the drug *in vitro* (Figure 1). The adductomic data-dependent constant neutral loss-MS^3 (DDA-CNL/MS^3) method can simultaneously screen for multiple DNA adducts by taking advantage of the common structural features of DNA adducts (the 2′-deoxyribose-nucleobase structure).[9,26,27] In this study, the neutral loss of the four nucleobase moieties (G, 151.0494 amu; A, 135.0545 amu; T, 126.0429 amu; and C, 111.0433 amu) and the 2′-deoxyribose moiety (116.0474 amu) were monitored and coupled with subsequent MS^3 fragmentation triggered upon neutral loss observation to gain additional structural characterization.

Using the DDA-CNL/MS^3 method, DNA hydrolysates of BU-treated and untreated CT-DNA were analyzed and compared. Data analysis was performed as previously reported, and ions corresponding to DNA adducts present only in the exposed sample were considered.[26] Briefly, scrutiny of the MS^2 and MS^3 spectra for each MS^3-triggering ion confirmed that the fragments observed resulted from a DNA adduct and were used to exclude any MS^3-triggering ions resulting from artifacts or false-positives. Specifically, for each ion, the MS^3 spectrum was scrutinized to (1) confirm the presence of one of the nucleobases and/or its fragments as product ions, and (2) evaluate that the accurate mass corresponding to the modification accounts for a realistic chemical formula. Furthermore, the precursor extracted ion chromatogram (EIC) was evaluated to confirm its peak-like shape and a minimum of four sticks across the peak. Finally, the retention times of the full scan, MS^2 and MS^3 spectra were evaluated to confirm that they coincided. Full-scan EICs for all candidate DNA adduct ions were generated for the exposed and unexposed samples, and only ions that were uniquely present in the exposed sample were annotated. Further confirmation was gained by evaluation of the presence of the adducts in both the ^{14}N and ^{15}N form when combining the analysis of ^{14}N- and ^{15}N-DNA exposed with BU.

A total of 20 compounds matching all the criteria were identified as putative BU-DNA adducts and listed in Table 1. The EIC for each of them is reported in Figure S2. As illustrated in Figure 2, a putative adduct with *m/z* 357.1530 shows a typical chromatogram with mass spectrometry (MS) traces of a clear full-scan peak aligning well with its MS^2 and MS^3 signals. The neutral loss of guanine observed in the MS^2 fragmentation, together with the appearance of the guanine ion $[Gua + H]^+$ in the MS^3 fragmentation suggests that this putative DNA adduct is likely to be a cross-link product of the drug with two guanine bases. We thus tentatively assign the structure of this adduct as *N*7G-Bu-*N*7G, **6** (Figure S1).

Confirmation of the putative BU DNA adducts using ^{15}N-labeled DNA

^{15}N-labeled *Escherichia coli* DNA is a useful tool to further confirm the putative BU-DNA adducts listed in Table 1.[29] A 1:1 mixture of unlabeled and ^{15}N-labeled *E. coli* DNA exposed to BU was hydrolyzed

Table 1. DNA adducts putatively identified in BU-treated calf-thymus DNA and the blood DNA of patients receiving BU therapy

$[M + H]^+$	tR (min)	NL	*E. coli* DNA (number of ^{15}N atoms)	Patient blood DNA[a]
224.1135	8.6	N	5	X
257.0880	8.6	dR	5	X
262.0860	18.0	C	–	X
264.6485	8.3	G	5	X
290.1724	8.2	G	5	X
298.1430	28.9	A	5	X
300.1401	29.0	A	5	X
302.0920	16.0	G	5	–
306.1560	6.4	dR	5	X
316.1349	34.5	G	10	–
357.1531	9.6	G	10	X
358.1276	17.7	dR	5	X
378.1330	17.9	dR	–	X
418.1390	15.0	dR	5	X
432.1823	28.3	dR	7	–
441.2218	8.2	G	5	X
449.1726	15.6	dR	10	X
465.2080	49.7	T	–	–
469.1782	15.6	dR	–	–
482.2170	49.9	T	–	–

[a]X indicates that adduct was detected in at least one patient.

and purified following the same approach described for the analysis of CT-DNA. The hydrolysate was analyzed by the same adductomic DDA-CNL/MS^3 method, with the exception that ^{15}N-labeled deoxyribonucleosides were included as monitored neutral losses. The acquired MS data were processed by the same approach described above. Only the peaks present in both ^{14}N- and ^{15}N-MS traces were considered as putative BU-DNA adducts, a representative example of which is shown in Figure 3. In this analysis, the presence of the two co-eluting peaks with *m/z* 357.1534 (unlabeled) and 367.1231 (^{15}N-labeled) agreed with the putative BU cross-link adduct **6** observed in Table 1 and Figure 2. The mass difference of 9.9703 amu (indicating 10 ^{15}N-labeled nitrogens) provides further evidence of forming the cross-link **6**, since each guanine contains five nitrogens.

We then manually excluded any peaks from the list of Table 1 (the column of unlabeled CT-DNA) that were not confirmed by the $^{14}N/^{15}N$ paired pattern in the BU-treated *E. coli* DNA. The number of putative BU-DNA adducts thus decreased to 15, as shown in Table 1. Insights on DNA adduct types were given by the mass difference between the $^{14}N/^{15}N$ paired peaks. As mentioned above, a mass difference of 4.9852 amu (corresponding to the adduct with five nitrogen atoms), indicates that the DNA adduct is a modification on a single Gua or Ade nucleobase (mono adduct). while a mass difference of 6.9890 or 9.9703 amu corresponds to a cross-link DNA adduct. Therefore, a total of four cross-links and 11 mono adducts are identified to be formed from BU treatment of DNA *in vitro*.

Targeted analysis of putative BU DNA adducts in the blood of patients

The presence of the putative BU-derived DNA adducts was investigated in the blood DNA of patients undergoing BU treatment. Blood samples were collected from six patients receiving BU therapy (Table 2). Samples were taken prior to the first administration (baseline sample) and within 24 h after the completion of the BU therapy (exposed sample). The paired blood DNA samples were analyzed using a targeted MS method for the 15 putative BU-DNA adducts (Table 1) observed *in vitro*. Twelve of the adducts were detected in at least one of the blood samples. Interestingly, two putative DNA adducts with *m/z* 357.1531 (tentatively assigned to be *N*7G-Bu-*N*7G, **6**) and 441.2218 (unknown) were present in all the six blood DNA samples of patients receiving BU therapy (Table S1). Some adducts, such as that with *m/z* 224.1135 (tentatively assigned to be *N*7G-Bu-OH, **7**) and 449.1726 (unknown), were also detected in five out of six patients. These results identified the BU adduct profile to be used to define the interaction of the drug with its molecular target in patients. These efforts led to the development of a quantitative/profiling method pairing the quantitation of the most common BU-derived DNA modifications, adducts **6** and **7,** with the profiling of all 15 detected putative DNA adducts.

Chemical synthesis of BU-derived DNA adducts

The synthesis of adducts **6** and **7** is illustrated in Figure S1. The same scheme was followed for the synthesis of their corresponding isotopically labeled analogs. The synthesis started with a common step in which the N^2-NH_2 of [$^{15}N_5$]2′-deoxyguanosine (dGuo) was first protected with the dimethylformamidine group to improve the regioselectivity of the alkylation reaction by 1,4-dibromobutane with **2**. This alkylation reaction requires nearly 2 weeks to complete (Figure S3) and room temperature stirring to achieve a better outcome. Then the intermediate **3** was reacted with excess **2** to yield the cross-link precursor **4**, which was easily converted to the final compound **6** via the NH_4OH-catalyzed deprotection reaction. During the cross-linking step, the bromine atom of **3** also underwent hydrolysis and formed the mono adduct precursor **5**. This precursor was readily converted to the mono adduct **7** by treatment with NH_4OH in MeOH. The same route was followed starting from [$^{15}N_5$]dGuo to obtain the corresponding isotopically labeled analogs of **6** and **7**.

Characterization of BU-derived DNA adducts

One critical aspect of the characterization of BU-derived DNA adducts **6** and **7** is to confirm the regioselective attack of the Gua-*N*7 position in the alkylation steps of Figure S1. During the first alkylation step, compound **3** was formed as the major product (Figure S3). As shown by Figure S4, the heteronuclear multiple bond correlations (HMBCs) between the methylene group (H1′) and the 5- and 8-carbons of the guanine base clearly demonstrate that the alkylation reaction is Gua-*N*7 selective under the mild conditions used. No such

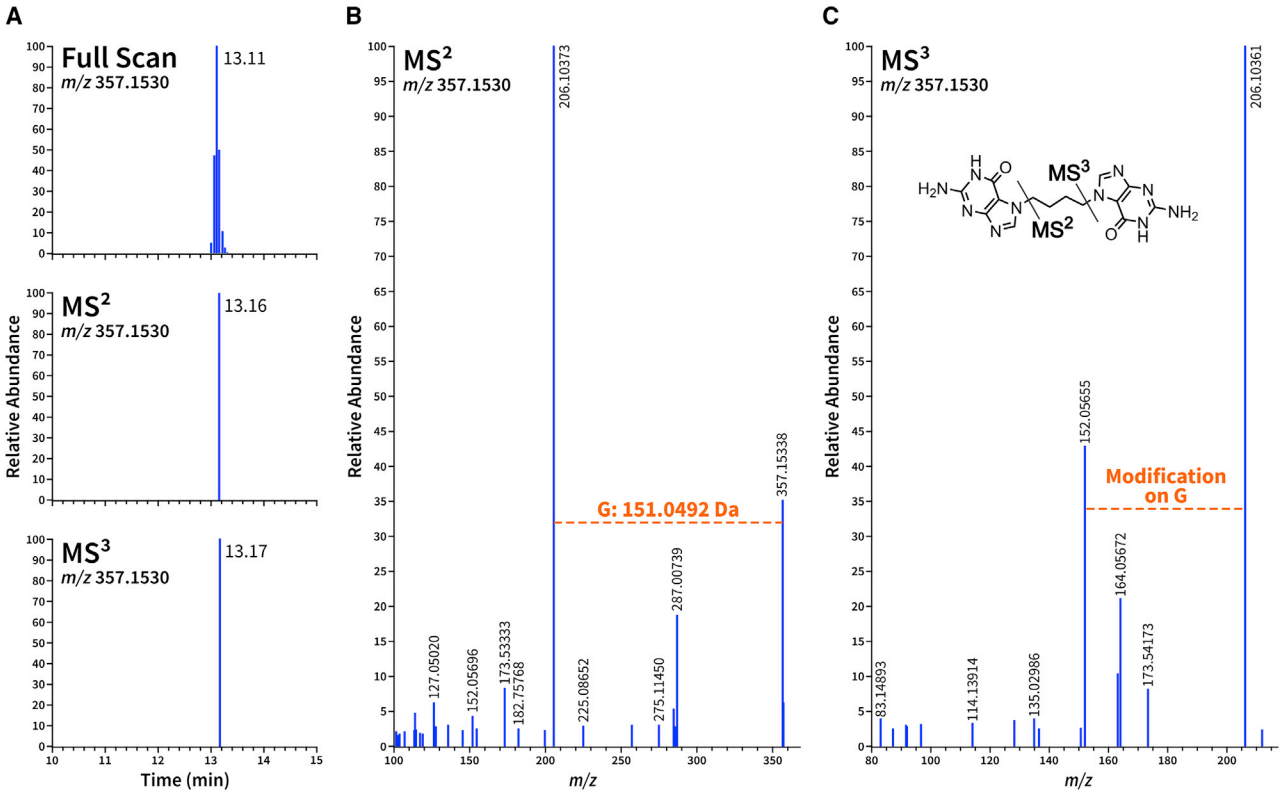

Figure 2. MS traces of EIC of *m/z* 357.1530 and its MS^2 and MS^3 fragmentation pattern in BU-treated CT-DNA

correlation is observed between the same methylene group and the 4-carbon of the guanine base. The full NMR characterization of compound **3** is also presented in Figure S4. The chemical structure of **7** is thus the Gua-*N7* alkylation product since the hydrolysis step and the deprotection step will not change the alkylation position.

For the structural assignment of the cross-link adduct **6**, additional HMBC evidence was needed for the second alkylation reaction by the intermediate **3** with **2**. As shown in Figure S5, correlations similar to those described for compound **3**, between the methylene group (H1′) and the Gua C5 and C8, were clearly observed. No signal was observed between the same methylene group and Gua C4 further supporting the structure of intermediate **4**. The full NMR characterization of this intermediate can also be found in the Figure S5. Similarly, the regioselectivity of the final cross-link **6** remains the same after the deprotection reaction from compound **4**.

The MS study of the synthesized standards provided convincing evidence for their structural assignments. MS fragmentation patterns of **6** and **7** both agreed with likely pathways. As shown in Figure 4, the major product ion of the cross-link adduct **6** is *m/z* 206.1033, which is the fragment ion resulting from the loss of a guanine; the major product ion of the mono adduct **7** is *m/z* 224.1138, which is the fragment ion resulting from the loss of the alkyl modification. The isotope-labeled chemical standards [$^{15}N_5$]**6** and [$^{15}N_5$]**7** eluted at the same high-pressure liquid chromatography (HPLC) retention time compared with the unlabeled adducts **6** and **7** in the BU-exposed CT-DNA (Figure 5). Their MS^2 fragmentation patterns were also identical to the unlabeled standards, with the most abundant product ions being *m/z* 211.0876 and 157.0412, respectively.

Quantification of *N*7G-Bu-*N*7G and *N*7G-Bu-OH in blood DNA of patients undergoing BU-based chemotherapy

The targeted HPLC-NSI-HRMS/MS method was used for the quantitation of the cross-link adduct **6** and the mono adduct **7** in the blood DNA of BU-exposed patients (Figure 6). The limit of detection (LOD) and limit of quantitation (LOQ) for adduct **6** were 0.015 and 0.05 fmol on-column, respectively; the LOD and LOQ for adduct **7** were 0.025 and 0.25 fmol on-column, respectively. Standard curves for both compounds were established by analyzing solutions containing a fixed amount of isotope-labeled adducts (**6**, 7.5 fmol; **7**, 5 fmol) mixed with increasing amounts of the unlabeled standards, followed by regression analysis of the calculated and experimentally determined relative response ratios (Figure 6). Solvent blanks were periodically injected to detect potential analyte carry-over. The concentration ranges for the calibration curves and validation experiments were chosen to cover the range of the levels of adducts found in human DNA samples. The calibration curves showed good linearity within the concentration ranges (R^2 = 0.99 for **6** and 0.98 for **7**). The assay accuracy was determined as a percentage of the added

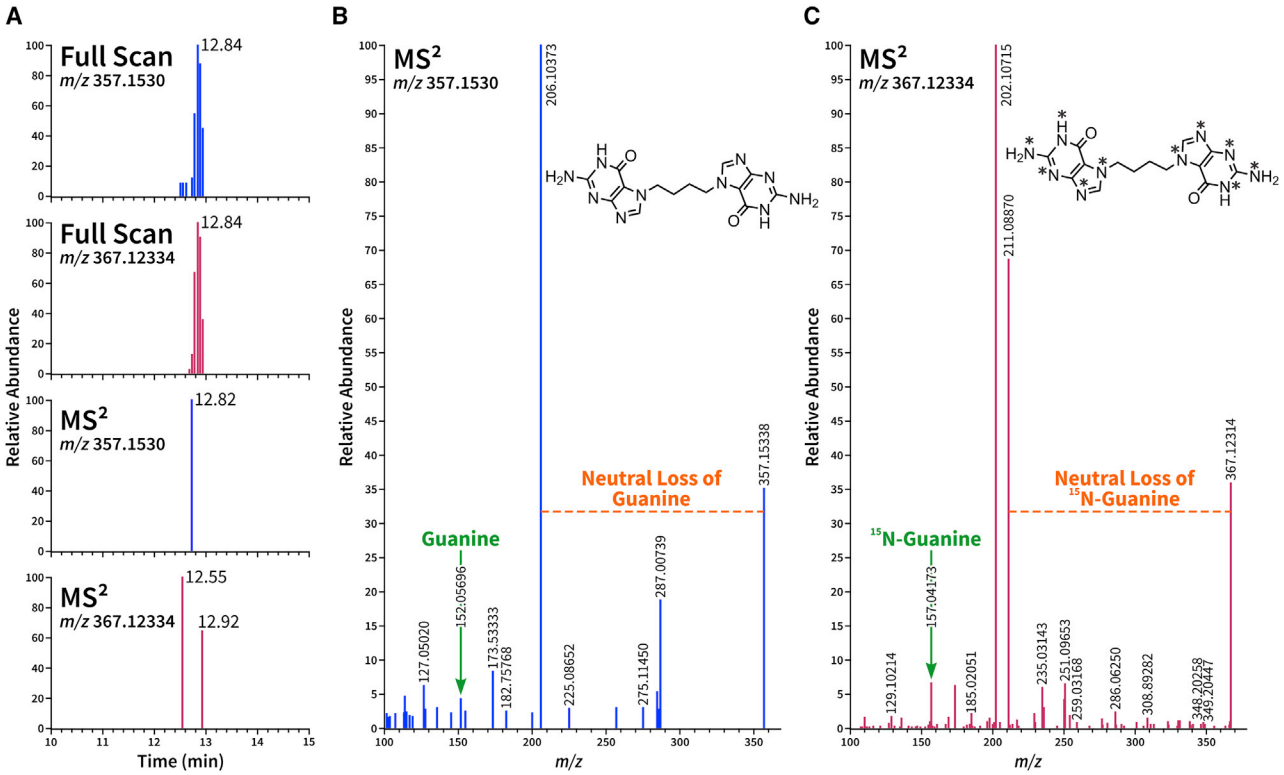

Figure 3. ^{15}N-DNA data for supporting DNA adducts characterization

(A) EIC of one detected adduct with *m/z* 357.1530, its ^{15}N-version *m/z* 367.1234, and the corresponding MS^2 scan events. (B) MS^2 spectra of the ion *m/z* 357.1530 and the hypothesized structure. (C) MS^2 spectra of the ion *m/z* 367.1233 and the hypothesized structure (ion *m/z* 202.1071 is not related to the molecule of interest).

amount of adducts to 20 μg of CT-DNA. The adducts were detected with excellent accuracies of 94% and 101.48% (n = 6) for **6** and **7**, respectively. Good linearity was also observed across the tested concentration ranges in the accuracy study. The precision of this assay was also satisfactory, with 6.9% for **6** and 7.6% for **7** by calculating the average of the coefficient of variation (CV) at each concentration of the curve. The total recoveries averaged 81% and 64% for **6** and **7** respectively.

As shown by Table 2, both the cross-link **6** and the mono adduct **7** were readily detected in most patients. The mono adduct **7** occurred in much higher abundance than the cross-link adduct **6**. The concentration of **7** was 6.8–20.6 times higher than that of **6** in each patient except for patient 4. A high interindividual variation was observed in the levels of adducts **6** and **7**. This may be due to the difference of total BU dose given to the patients, to interindividual difference in forming and repairing DNA adducts, or to a combination of both.

DISCUSSION

In this study, we characterized for the first time BU-derived DNA adducts in the blood of HCT patients receiving this therapy. Twelve out of 15 putative DNA adducts observed *in vitro* were detected in patients. Two of them were characterized to be the cross-link DNA adduct **6** and the mono DNA adduct **7**. A quantitative method for the analysis of these two adducts was developed to be combined with the screening analysis for all other BU-derived DNA modifications identified here. This study provides a promising approach to develop predictive biomarkers for future use to monitor the effects of BU and support personalized therapies.

The mechanism of action for DNA alkylating drugs such as BU is their ability to damage DNA. However, this interaction can also result in therapy toxicities, especially when high-dosage treatment is required.[5] On the other hand, low doses of alkylating drugs result in insufficient cancer cell DNA damage, which has been associated with drug resistance and therapy failure.[5] A fine balance needs to be found to administer these drugs at appropriate concentrations. Furthermore, patient-specific aspects, such as DNA repair mechanisms or drug metabolisms, are variables that may dramatically influence the generation of DNA damage and therefore the efficacy of the treatment. A profile of BU-derived DNA adducts provides integrated information on the drug activity and individual variables that may influence it and therefore is an excellent candidate as a predictive biomarker in precision oncology.[5]

There are limited studies showing the addition products of BU with glutathione.[30–32] Scian and coworkers studied the role of BU-related metabolite γ-glutamyldehydroalanylglycine (EdAG) and the action

Table 2. Diagnosis, sex, and levels of DNA adducts 6 and 7 in patients receiving BU-based chemotherapy

Patient	Diagnosis	Sex	*N*7G-Bu-*N*7G (**6**) Adducts/10^6 nucleosides	*N*7G-Bu-OH (**7**) Adducts/10^6 nucleosides
1	Acute myeloid leukemia	F	0.62	12.8
2	Acute myeloid leukemia	F	1.54	26.7
3	Fanconi anemia	F	0.38	ND
4	Multiple sulfatase deficiency	F	2.02	13.7
5	Acute myeloid leukemia	F	0.62	28.2
6	Fanconi anemia	M	1.60	26.3

DNA modifications derived from the alkylating drug BU were profiled with our novel adductomics approach *in vitro*. The detected adducts were investigated in patients undergoing BU-based chemotherapy, two of which were chemically characterized and quantified. This study sets the stage for the evaluation of BU adducts for therapy personalization.

of BU on intact proteins, highlighting novel mechanisms of BU toxicity.[33–35] However, to the best of our knowledge, no study has characterized DNA adducts formed by BU. Iwamoto and coworkers demonstrated that BU caused DNA damage at 5′-GA-3′ and 5′-GG-3′ sequences *in vitro* with detection of two structurally unknown adducts.[25] They concluded that the generation of cross-links may be a strong mechanism of BU cytotoxicity. Souliotis and colleagues highlighted the relevance of mono adducts in therapeutic effect, supporting a two-step mechanism of generation of cross-linked adducts. Indeed, cross-links may be generated by a delayed binding to a second site in DNA.[36] Therefore, repair of mono adducts may interfere with the generation of cross-linked adducts and module the drug cytotoxicity.[36] Interstrand lesions are thought to play a central role in the cytotoxic response because they prevent DNA strand separation, which is required for DNA replication and transcription.[37] Overall, these observations support the importance of monitoring the full profile of adducts rather than focusing only on few major ones. Traditionally, the interactions between alkylating drugs and nucleic acids have been studied by targeting a few specific analytes resulting from the main chemical modifications occurring according to the known reactivity of the drug with DNA's reactive sites. Our novel DNA adductomics approach, instead, allows the simultaneous screening of all DNA covalent modifications (not only the major ones), including both known and previously unidentified ones. This more comprehensive method may also include those resulting from metabolic modifications or activation pathways that may be unexpected. The possibility to screen how the drug, directly or through its metabolites, interacts with DNA gives a full picture of all the possible interactions of the drug and the metabolites with their target. In addition to the direct action of drug with DNA, this allows us to understand the role of all the metabolic processes involved. Furthermore, different DNA modifications may be affected by DNA repair mechanisms in various ways and at different rates, thus screening for multiple DNA adducts allows us to potentially monitor the influence of repairing enzymes on the action of the drug.

In the present study, we first investigated the formation of BU-DNA adducts in our *in vitro* samples with BU-exposed CT-DNA and ^{14}N-/^{15}N-DNA mixture from *E. coli*, and identified four putative cross-links including adduct **6** and 11 mono adducts including adduct **7**. Since the synthesis and characterization of all adducts would require enormous effort, we focused on the development of a quantitative method for the two major adducts **6** and **7** in the profile, namely those that were present in most samples. In the future, these two adducts will serve as standards for the development of analytical methods aimed at profiling all DNA adducts and evaluating their relationship with patient outcome.

The chemical synthesis of **6** and **7** was pursued for absolute characterization and development of a quantitative method to be used in parallel to the profiling. The synthetic strategy for synthesizing the cross-link adduct **6** utilized two sequential alkylation reactions instead of the classical method of treating dGuo with the alkylating agent (such as nitrogen mustard[3] and bis(2-chloroethyl)ethylamine[38]) in a one-step reaction. The advantages of our method are (1) allowing a full NMR characterization of the Gua-*N*7-alkyl product obtained from each alkylation reaction, and (2) yielding cleaner reaction mixtures for a better separation of the desired product. We failed to identify desired products from the reaction mixture of dGuo with BU or 1,4-dibromobutane due to the complexity of the HPLC traces.

The success of the first-step alkylation (Figure S1) is critical. This reaction requires a long reaction time (14 days) with mild stirring at room temperature to achieve completion (Figure S3). Increasing the reaction temperatures (e.g., 60°C) or use of different solvents (e.g., DMSO) and added bases (e.g., Et_3N, DBU, K_2CO_3) failed to facilitate the reaction; all the reactions yielded much more complex products with no improved yields of the desired product **3**. For the second-step alkylation, the reaction yield for compound **4** is very low even with excess starting material **2**. The product **5** is considered the hydrolysis product from **3** during the second-step alkylation reaction in a similar low yield. The mild condition from the first-step alkylation reaction did not work for the second-step alkylation, even after up to 14 days. One important observation is that the excess amount of NH_4OH used for the deprotection reaction of **4** could degrade the product **6** but did not appear to affect compound **7**.

Using the synthesized standards, we were able for the first time to quantify BU-derived DNA adducts in patients. The concentrations of **7** ranged from 12.8 to 28.2 adducts/10^6 nucleotides (except for patient 3), significantly higher than those of **6**, which ranged from 0.38 to 2.02 adducts/10^6 nucleotides. Out of the 15 putative DNA adducts detected *in vitro*, 12 were detected in at least one patient undergoing BU-based chemotherapy. Interestingly, several DNA adducts are in common among patients underlining a general reaction mechanism between BU and DNA. Chemical modifications to guanine and adenine are observed to be the most frequent ones as commonly reported in past investigations of alkylating drugs.[3,36,38,39] An isotope

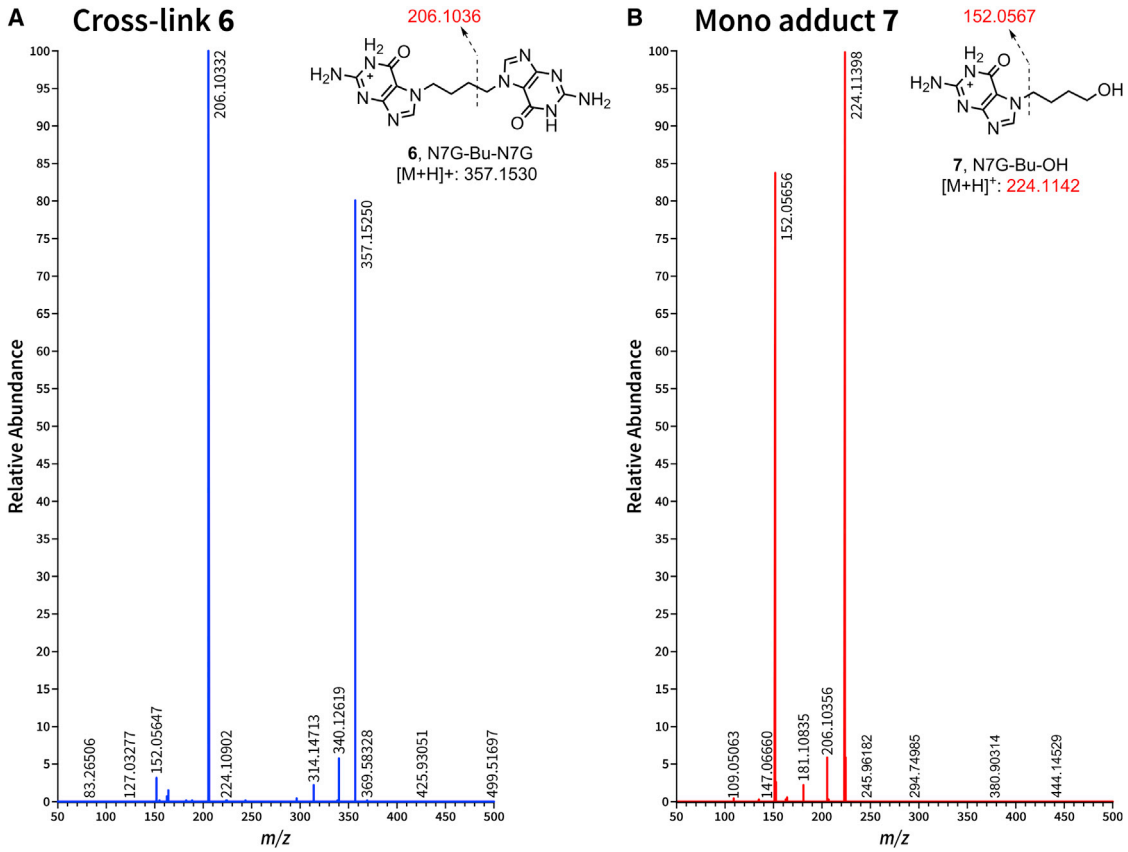

Figure 4. Mass spectra of synthetic standards
HRMS analysis of synthetic standards of cross-link **6** (A) and mono adduct **7** (B).

dilution method was developed and validated for quantifying the cross-link adduct **6** and the mono adduct **7**. The cross-link adduct **6** and the mono adduct **7** were formed at high levels, ranging from 0.3 to 2 and from 1 to 263 adducts every 10^6 nucleosides, respectively. The higher amount of the mono adduct is consistent with the observations of Soulioti et al., Palom et al., and Hemminki in the cases of cyclophosphamide and mitomycin exposure.[36,39,40] However, due to the small number of patients in the present study with different doses and imprecise therapy time courses, the evaluation of the effects of adducts **6** and **7** on therapeutic outcome was not possible but can be done in the future.

In conclusion, we explored for the first time the BU-DNA adductome using a DNA adductomic approach. This resulted in a list of 15 putative DNA adducts formed by BU treatment in CT-DNA. Twelve of the 15 adducts were detected in the blood DNA of six patients undergoing BU treatment, and two of these were characterized to be the cross-link DNA adduct **6** and the mono DNA adduct **7** by comparison with their corresponding synthesized standards. An isotope dilution HPLC-NSI-HRMS/MS method was developed to quantify the two adducts in the blood DNA. Their formation occurred in relatively high concentrations, suggesting their potential as promising biomarkers for the investigation of interindividual differences in BU-induced DNA adducts for patient stratification.

MATERIALS AND METHODS

Chemicals and supplies

Methanol (MeOH, liquid chromatography [LC]-MS grade), acetonitrile (ACN, LC-MS grade), isopropanol (IPA), and formic acid (FA, 98% $_{v/v}$) were purchased from Fluka (St. Louis, MO, USA). Water was purified by a Milli-Q system (Milford, MA, USA). Cell Lysis Solution, Proteinase K, and RNase-A were purchased from Qiagen (Germantown, MD, USA). DNase I recombinant expressed by *Pichia pastoris* (R-DNase, 10,000 U/mg), phosphodiesterase-1 extracted from *Crotalus adamanteus* (PDE-1, 0.4 U/mg), recombinant alkaline phosphatase expressed by *P. pastoris* (R-ALP, 7,000 U/mg), and calf-thymus DNA (CT-DNA) were purchased from Roche (St. Louis, MO, USA). Single-membrane filtration devices Microcon (10-kDa cutoff, 0.5 mL) were purchased from Amicon (Billerica, MA, USA). Silanized vials (0.3, 1.2, and 4 mL) were purchased from ChromTech (Apple Valley, MN, USA). [$^{15}N_5$]2′-deoxyguanosine (dGuo) was purchased from Cambridge Isotope Laboratories. All other chemicals and supplies were purchased from Sigma-Aldrich or Fisher Scientific.

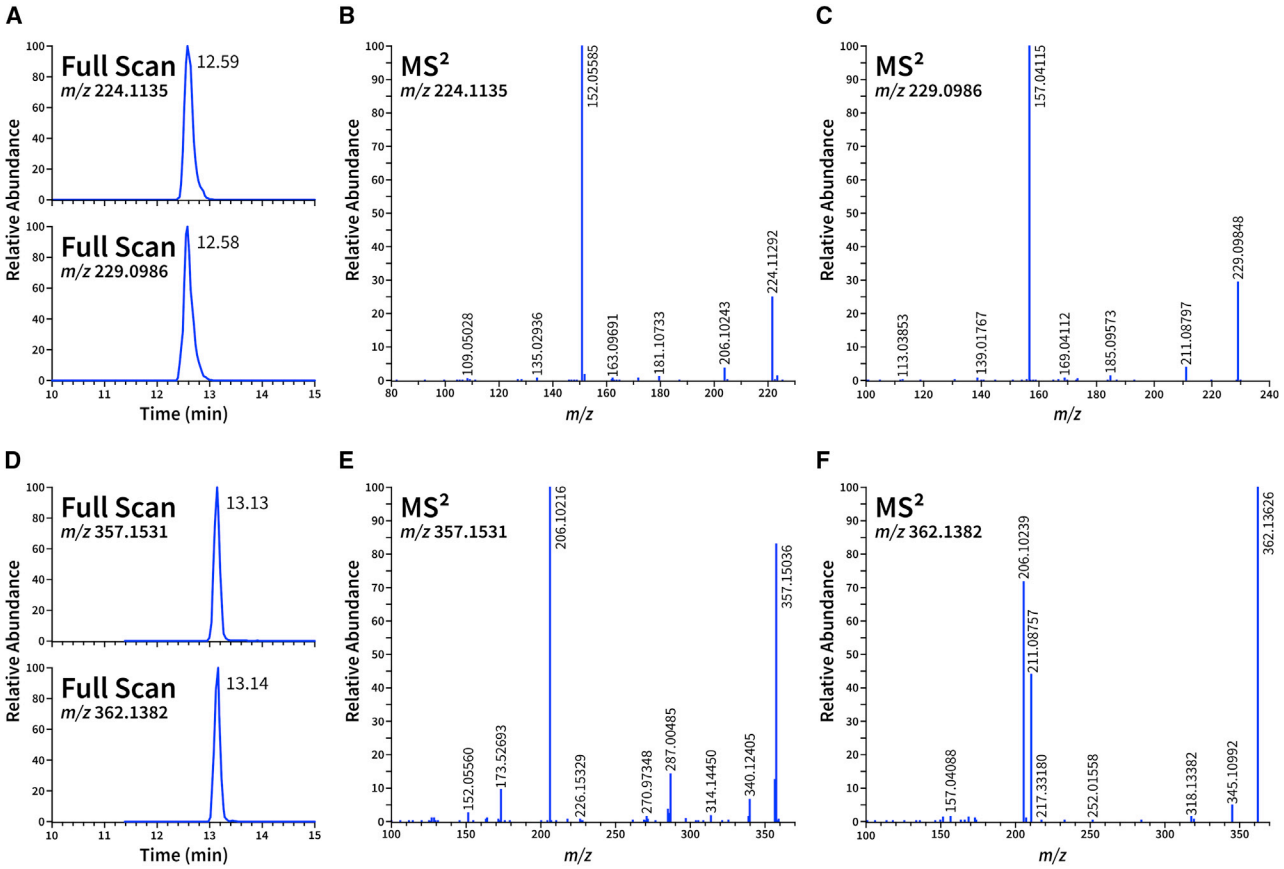

Figure 5. Chromatograms resulting from co-injection of standards with the CT-DNA sample exposed to BU for analyte confirmation
(A) EIC of *m/z* 224.1135 and 229.0986. (B and C) Relative MS^2 spectra. (D) EIC of *m/z* 357.1531 and 362.1382. (E and F) Relative MS^2 spectra.

Synthesis of chemical standards

N'-(9-((2R,4S,5R)-4-hydroxy-5-(hydroxymethyl)tetrahydrofuran-2-yl)-6-oxo-6,9-dihydro-1H-purin-2-yl)-N,N-dimethylformimidamide (2, N^2-dmf-dGuo)

N,*N*-dimethylacetamide dimethyl acetal (2.0 mL) was added to a solution of dGuo (3.5 mmol, 1.0 g) in MeOH (9.5 mL). The reaction mixture was stirred at room temperature for 3 days. After reaction, the precipitated white solid was filtered and washed with cold MeOH. The solid was dried and used directly without further purification (1.05 g, 93%). ^{1}H NMR (500 MHz, DMSO-d_6) δ 11.31 (s, 1H, H1), 8.55 (s, 1H, $(CH_3)_2NC\underline{H}$ = N-), 8.03 (s, 1H, H8), 6.25 (dd, *J* = 7.9, 6.1 Hz, 1H, H1′), 5.29 (d, *J* = 3.9 Hz, 1H, 3′-OH), 4.93 (t, *J* = 5.5 Hz, 1H, 5′-OH), 4.37 (dq, *J* = 6.1, 3.0 Hz, 1H, H3′), 3.83 (td, *J* = 4.6, 2.5 Hz, 1H, H4′), 3.57 (dt, *J* = 11.7, 5.1 Hz, 1H, H5′a), 3.51 (ddd, *J* = 11.6, 5.8, 4.4 Hz, 1H, H5′b), 3.16 (s, 3H, -CH_3), 3.03 (s, 3H, -CH_3), 2.59 (ddd, *J* = 13.5, 8.0, 5.7 Hz, 1H, H2′a), and 2.23 (ddd, *J* = 13.2, 6.1, 2.9 Hz, 1H, H2′b). For the synthesis of the isotopically labeled compound [$^{15}N_5$]**2**, *N*,*N*-dimethylacetamide dimethyl acetal (1.0 mL) was added to a solution of [$^{15}N_5$]dGuo (5.0 mg, 0.018 mmol) in MeOH (1.0 mL). After stirring at room temperature for 3 days, the reaction mixture was dried to remove most of the solvent and diluted with H_2O (0.5 mL) before performing reverse-phase HPLC purification using Waters Associates (Milford, MA) systems equipped with a Shimadzu SPD-10A 0.2 mm Prep UV-vis detector (254 nm). A Luna 5-μm C18(2) 100 Å 250 × 10-mm column purchased from Phenomenex (Torrance, CA) was used for the separation. A 50-min program was used with a flow rate of 4 mL/min and a gradient starting from 5% MeOH in H_2O for 10 min, then increasing linearly to 90% MeOH in H_2O over 25 min. After holding at 90% MeOH in H_2O for 3 min, the gradient was returned to the initial condition of 5% MeOH in H_2O over 5 min. The system was equilibrated for 7 min before the next injection. The desired product [$^{15}N_5$]**2** was collected at the retention time of 22 min ^{1}H NMR (500 MHz, MeOD) δ 8.64 (d, *J* = 2.3 Hz, 1H, $(CH_3)_2NC\underline{H}$ = ^{15}N-), 8.06 (dd, *J* = 11.3, 7.8 Hz, 1H, H8), 6.37 (ddd, *J* = 7.7, 6.1, 1.4 Hz, 1H, H1′), 4.55 (dt, *J* = 6.1, 3.0 Hz, 1H, H3′), 4.01 (q, *J* = 3.5 Hz, 1H, H4′), 3.79 (dd, *J* = 12.0, 3.6 Hz, 1H, H5′a), 3.72 (dd, *J* = 12.0, 3.9 Hz, 1H, H5′b), 3.21 (s, 3H, -CH_3), 3.12 (s, 3H, -CH_3), 2.73 (dddd, *J* = 13.6, 8.3, 6.1, 2.7 Hz, 1H, H2′a), and 2.39 (dddd, *J* = 13.5, 6.2, 3.2, 1.3 Hz, 1H, H2′b).

N'-(7-(4-bromobutyl)-6-oxo-6,7-dihydro-1H-purin-2-yl)-N,N-dimethylformimidamide (3, N^2-dmf-Gua-N7-butylbromide)

A solution of **7** (0.5 mmol, 161 mg) and 1,4-dibromobutane (2.5 mmol, 300 μL) in *N*,*N*-dimethylformamide (DMF, 2.0 mL) was

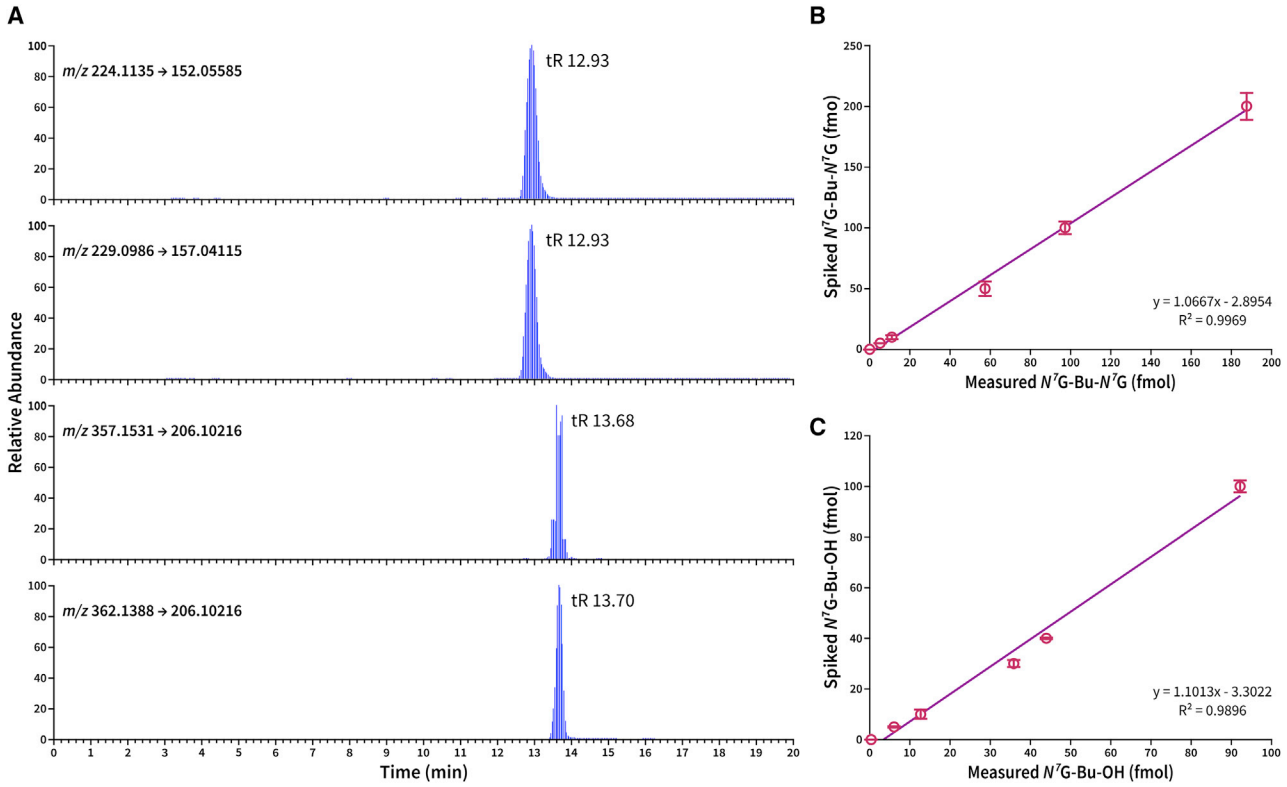

Figure 6. Example of DNA adduct detection in patients and calibration curves

(A) Representative EIC of respectively adduct **6**, its internal standard and **7**, and relative internal standard in patient DNA. (B and C) Measured and spiked amount of adducts **6** and **7** for method validation. Error bars for measures repeated in triplicates (n=3).

stirred at room temperature for 14 days. The reaction mixture turned from a white suspension to a clear yellow solution after 8 days. After completion, the reaction mixture was subjected directly to reverse-phase HPLC for purification using the same conditions described for the synthesis of [$^{15}N_5$]**2**. The desired product **3** eluted at 30.4 min as the major peak (Figure S3). After drying under a stream of N_2, compound **3** was collected as a white solid (101 mg, 60%). The full NMR spectra are presented in Figure S4. ^{1}H NMR (500 MHz, DMSO-d_6) δ 11.34 (s, 1H, H1), 8.60 (s, 1H, $(CH_3)_2NCH$ = N-), 8.01 (s, 1H, H8), 4.26 (t, J = 6.7 Hz, 2H, -$CH_2CH_2CH_2CH_2Br$), 3.53 (td, J = 6.7, 2.2 Hz, 2H, -$CH_2CH_2CH_2CH_2Br$), 3.14 (s, 3H, -CH_3), 3.01 (s, 3H, -CH_3), 1.96–1.86 (m, 2H, -$CH_2CH_2CH_2CH_2Br$), 1.79–1.66 (m, 2H, -$CH_2CH_2CH_2CH_2Br$). ^{13}C NMR (126 MHz, DMSO) δ 158.90 (C4), 157.64 ($(CH_3)_2NCH$ = N-), 156.45 (C2), 155.27 (C6), 143.40 (C8), 110.70 (C5), 45.12 (-$CH_2CH_2CH_2CH_2Br$), 40.46 (-CH_3), 34.51 (-CH_3), 34.30 (-$CH_2CH_2CH_2CH_2Br$), 29.24 (-$CH_2CH_2CH_2CH_2Br$), and 29.06 (-$CH_2CH_2CH_2CH_2Br$). HRMS (Orbitrap): $[M + H]^+$ calculated (calc'd) 341.0720, 343.0700; 286.0298, 288.0278; found 341.0665, 343.0641; 286.0329, 288.0310. For the synthesis of the isotopically labeled compound [$^{15}N_5$]**3**, 1,4-dibromobutane (20 μL) was added to a solution of [$^{15}N_5$]**2** in DMF (0.5 mL). The reaction mixture was stirred at room temperature for 14 days. After reaction, the reaction mixture was subjected directly to reverse-phase HPLC, and the desired product [$^{15}N_5$]**3** was collected at the retention time of 30.3 min under the same conditions described for the synthesis of [$^{15}N_5$]**2**. HRMS (Orbitrap): $[M + H]^+$ calc'd 346.0572, 348.0552; 291.0150, 293.0130; found 346.0578, 348.0648; 291.0343, 293.0314.

N',N''-(butane-1,4-diylbis(6-oxo-6,7-dihydro-1H-purine-7,2-diyl)) bis(N,N-dimethylformimidamide) (4, bis(N^2-dmf-Gua-N7)butyl, and N'-(7-(4-hydroxybutyl)-6-oxo-6,7-dihydro-1H-purin-2-yl)-N,N-dimethylformimidamide (5, N^2-dmf-Gua-N7-butanol)

To a solution of **3** (0.22 mmol, 101 mg) in DMF (1.5 mL), compound **2** (0.29 mmol, 94 mg) was added. The reaction mixture was stirred at 60°C for 2 days and then analyzed by reverse-phase HPLC directly under the same conditions described for the synthesis of [$^{15}N_5$]7. The desired products **4** and **5** were collected at 25.6 and 26.0 min, respectively, in very low yields (<1%) (Figure S6). The isotopically labeled compounds [$^{15}N_5$]**4** and [$^{15}N_5$]**5** were synthesized in the same way as **4** and **5**. A solution of **2** (16.2 mg, 0.05 mmol) was added to a DMF (0.5 mL) solution of [$^{15}N_5$]3. The reaction mixture was stirred at 60°C for 2 days. After reaction, the resulting mixture was subjected to reverse-phase HPLC directly using the same separation conditions as described above. The desired compounds [$^{15}N_5$]**4** and [$^{15}N_5$]**5** were collected at the retention times of 25.6 and 26.0 min, respectively.

Compound **4** was fully characterized by one- and two-dimensional NMR and HRMS. The NMR spectra are presented in Figure S5. ^{1}H NMR (500 MHz, MeOD) δ 8.59 (s, 2H, $(CH_3)_2NCH$ = N-), 7.99 (s, 2H, H8), 4.48–4.30 (m, 4H, N-CH_2CH_2-), 3.18 (s, 6H, -CH_3), 3.10 (s, 6H, -CH_3), 2.18–1.69 (m, 4H, N-CH_2CH_2-). ^{13}C NMR (126 MHz, MeOD) δ 160.50 (C4), 159.44 ($(CH_3)_2NCH$ = N-), 158.85 (C2), 144.92 (C8), 112.03 (C5), 47.45 (N-CH_2CH_2-), 41.29 (-CH_3), 35.16 (-CH_3), and 28.84 (N-CH_2CH_2-). HRMS (Orbitrap): $[M + H]^+$ calc'd 467.2374; found 467.2359. However, parent is in lower abundance than its fragment *m/z* 266.1310. The structure of $[^{15}N_5]$**4** was confirmed by HRMS. HRMS (Orbitrap): $[M + H]^+$ calc'd 472.2226, 266.1310, 261.1458; found 266.0663 and 261.2174 (no parent mass was observed, as above noted due to in-source fragmentation and spontaneous loss of Boc group in the source).

Compound **5** was characterized by ^{1}H NMR (Figure S7) and HRMS. ^{1}H NMR (500 MHz, MeOD) δ 8.61 (s, 1H, $(CH_3)_2NCH$ = N-), 8.07 (s, 1H, H1), 8.01 (s, 1H, H8), 4.37 (t, *J* = 7.1 Hz, 2H, -$CH_2CH_2CH_2CH_2$OH), 4.18 (t, *J* = 6.4 Hz, 2H, -$CH_2CH_2CH_2CH_2$OH), 3.19 (s, 3H, -CH_3), 3.11 (s, 3H, -CH_3), 1.99 (p, *J* = 7.3 Hz, 2H, -$CH_2CH_2CH_2CH_2$OH), and 1.68 (dt, *J* = 14.1, 6.6 Hz, 2H, -$CH_2CH_2CH_2CH_2$OH). HRMS (Orbitrap): $[M + H]^+$ calc'd 279.1564; found 279.1573. The structure of $[^{15}N_5]$**5** was confirmed by HRMS. HRMS (Orbitrap): calc'd $[M + H]^+$ 284.1416; found 284.1414.

7,7′-(Butane-1,4-diyl)bis(2-amino-1,7-dihydro-6H-purin-6-one) (6, N7G-Bu-N7G)

To a solution of **4** (∼1 mg) in MeOH (0.5 mL) was added 28%–30% NH_4OH solution (0.1 mL). The reaction mixture was stirred at room temperature overnight. After completion, the reaction mixture was dried by a stream of N_2 and the residue was reconstituted in H_2O before subjecting it to reverse-phase HPLC for purification using the same conditions described for the synthesis of $[^{15}N_5]$**2**. The desired product **6** was eluted at 21.1 min (Figure S8). The ^{1}H NMR spectra are presented in Figure S8. ^{1}H NMR (500 MHz, MeOD) δ 7.69 (s, 2H, H8), 4.31 (t, *J* = 6.8 Hz, 4H, N-CH_2CH_2-), 4.08 (t, *J* = 6.9 Hz, 4H, N-CH_2CH_2-). ^{1}H NMR (500 MHz, DMSO-d_6) δ 7.63 (s, 2H, H8), 4.20 (t, *J* = 6.4 Hz, 4H, N-CH_2CH_2-), and 3.92 (t, *J* = 6.8 Hz, 4H, N-CH_2CH_2-). HRMS (Orbitrap): $[M + H]^+$ calc'd 357.1530; found 357.1525. The isotopically labeled compound $[^{15}N_5]$**6** was synthesized using the same method used for **6**. To a solution of $[^{15}N_5]$**4** in MeOH (0.5 mL) was added 28%–30% NH_4OH solution (0.1 mL), and the mixture was stirred at room temperature overnight. After reaction, the solvent was removed by drying with a stream of N_2 and the residue was reconstituted in H_2O before subjecting it to reverse-phase HPLC for purification using the same conditions described for the synthesis of $[^{15}N_5]$**2**. The desired product $[^{15}N_5]$**6** was collected at 21.2 min. The structure of $[^{15}N_5]$**6** was confirmed by HRMS. HRMS (Orbitrap): $[M + H]^+$ calc'd 362.1382; found 362.1382.

2-Amino-7-(4-hydroxybutyl)-1,7-dihydro-6H-purin-6-one (7, N7G-Bu-OH)

Compound **7** and its isotopically labeled analog $[^{15}N_5]$**7** were synthesized similarly as compound **6**. The desired product **7** eluted from HPLC at 20.1 min (Figure S9) under the same conditions described for the synthesis of $[^{15}N_5]$**2**. The desired product $[^{15}N_5]$**7** was collected at 20.0 min. The structure of compound **7** was confirmed by ^{1}H NMR (Figure S9) and HRMS. ^{1}H NMR (500 MHz, DMSO) δ 10.70 (s, 1H, H1), 7.89 (s, 1H, H8), 6.07 (s, 2H, N^2-NH_2), 4.41 (t, *J* = 5.2 Hz, 1H, -OH), 4.17 (t, *J* = 6.9 Hz, 2H, -$CH_2CH_2CH_2CH_2$OH), 1.77 (p, *J* = 7.1 Hz, 2H, -$CH_2CH_2CH_2CH_2$OH), and 1.32 (dt, *J* = 14.1, 6.6 Hz, 2H, -$CH_2CH_2CH_2CH_2$OH). HRMS (Orbitrap): $[M + H]^+$ calc'd 224.1142; found 224.1141. The structure of $[^{15}N_5]$**7** was confirmed by HRMS. HRMS (Orbitrap): $[M + H]^+$ calc'd 229.0994; found 229.0993.

DNA isolation and purification

^{15}N-DNA generation

E. coli (MG1655 strain) was cultured in ^{15}N-labeled minimal medium (5 mL) at 37°C overnight for three generations to obtain a uniformly labeled ^{15}N-strain. The optical density 600 (OD_{600}) was used to monitor bacterial growth until stationary phase. The bacteria culture was centrifuged at 3,000 × *g* for 10 min at 24°C. The bacterial pellet was re-suspended in 50% glycerol in bacterial medium solution, frozen, and stored at −80°C until use. ^{15}N-labeled minimal medium (1 L) was prepared using 200 mL of M9 salts ($Na_2HPO_4 \cdot 7H_2O$, 64 g KH_2PO_4, 15 g, NaCl, 2.5 g, and $^{15}NH_4Cl$, 5.0 g in deionized H_2O, 1 L), and added to 20 mL of glucose (20%; Sigma-Aldrich), 2 mL of $MgSO_4$ (1 M; Fisher Scientific), and 100 μL of $CaCl_2$ (1 M; Fisher Scientific). A starter culture was prepared by inoculating 10 μL of ^{15}N- and ^{14}N-stock bacteria into 5 mL of medium and grown overnight. Fifty microliters of cells were then inoculated in 1 L of medium and incubated overnight. Cells were centrifuged and the pellet stored at −80°C until use (Figure S10).

Bacterial DNA isolation

Cells were re-suspended in 25 mL of Cell Lysis Solution (Qiagen) and treated with 150 μL each of Proteinase K (24 h, 24°C) and RNase-A (2 h, 24°C). Proteins were precipitated by adding 7.5 mL of Protein Precipitation Solution (Qiagen). The pellet was discarded and the supernatant was transferred into a new tube containing an equal amount of cold isopropanol (IPA) to precipitate the DNA. The mixture was centrifuged, the supernatant was discarded, and the DNA pellet was sequentially washed with 70% (v/v) IPA in H_2O and 100% IPA. The DNA pellet was dried, re-suspended in buffer (20 mM Tris, 2 mM $MgCl_2$ pH 7.4), and stored at −20°C. The yield and purity of the DNA were assessed using a nanodrop UV-visible (UV-vis) spectrophotometer monitoring the 260- and 280-nm wavelengths.

Sample collection from patients and whole-blood DNA extraction

This study was approved by the University of Minnesota Institutional Review Board (IRB) (no. 1506M74263). All patients signed IRB-approved informed consent in accordance with the Declaration of Helsinki. Blood (∼3 mL) was obtained from four cancer and two Fanconi Anemia patients undergoing allogeneic HCT receiving BU as part of their preparative regimens. Patients received a 2-h infusion of intravenous BU prior to their HCT. Whole blood was obtained

from a central venous catheter immediately prior to the first dose of BU (0 h) and within 24 h after the completion of the BU infusion protocol for a total of six baseline samples to be compared with the matching six samples post treatment. Whole-blood DNA extraction was performed immediately after the sample collection. Whole-blood DNA extraction was performed using Qiagen DNA extraction kits (Qiagen, Valencia, CA) by the manufacturer's instructions with slight modifications as previously reported.[41] DNA amounts were estimated by UV and subsequently determined by HPLC analysis of dGuo in enzymatic hydrolysates as described below. DNA samples (10–50 μg in 200 μL of Tris buffer) were spiked with 30 fmol of [$^{15}N_5$]*N*7G-Bu-OH and 50 fmol of [$^{15}N_5$]*N*7G-Bu-*N*7G as internal standards and subjected to enzymatic hydrolysis as described below.

DNA exposure to BU in vitro

CT-DNA (100 μg) or ^{14}N- and ^{15}N-bacterial DNA (210 μg each; 1:1 ratio) was dissolved in Tris buffer (20 mM Tris, 2 mM $MgCl_2$, pH 7.4). BU (in DMSO) was added to the DNA solutions separately to reach a final concentration of 100 μM (246 ng/mL) in each batch. This is close to the levels measured in patient plasma of previous studies.[42] The total volume of the corresponding sample was 200 μL. The resulting mixture was incubated at 37°C overnight. DNA exposed to DMSO (1% v/v) was used as a negative control. DNA isolation was performed by IPA precipitation. Briefly, 1 mL of cold IPA was added to each sample vial. The precipitated DNA was isolated, washed sequentially with 1 mL each of 70% IPA and 100% IPA twice, and dried under a stream of N_2. All steps of the protocol were performed using silanized glass vials.

DNA hydrolysis and sample enrichment

DNA enzymatic hydrolysis

DNA obtained above was dissolved in Tris buffer and incubated with R-DNase (0.5 U/μg DNA) at room temperature overnight. The following day, an additional amount of R-DNase (0.5 U/μg DNA) and R-ALP-1 (0.4 U/μg DNA) and PDE-1 (0.02 mU/μg DNA) were added and the mixture was incubated at 37°C for 70 min. The mixture was further incubated at room temperature overnight. After hydrolysis, enzymes were removed via filtration (Microcon, 10-kDa cutoff) by centrifuging at 12,000 × *g* for 60 min. The filtrate was collected for the analyte analysis and dGuo quantitation.

dGuo quantitation by HPLC

Quantitation of dGuo was carried out using a Dionex UltiMate 3000 RSLCnano System (Thermo Scientific, Waltham, MA) with a UV detector set at 254 nm. A 300-μm internal diameter (ID) × 15-cm C18 column (2 μm, 100 Å) (Thermo Scientific, Waltham, MA) was used with (A) H_2O and (B) MeOH as the mobile phase. The injection volume was 1 μL and the flow rate was 15 μL/min. Starting from 5% B for 2 min, a linear gradient was applied increasing from 5% to 25% B in 10 min. The gradient increased to 95% B in 3 min and was held for 5 min before returning back to the initial condition in 2 min. The instrument was equilibrated for 3 min (25 min total run time) before the next injection. A calibration curve for dGuo (0.0625–50 ng/μL in H_2O) was run in triplicate and used to calculate the dGuo content in each sample.[43]

Sample enrichment and purification

DNA hydrolysates were partially purified by solid-phase extraction using Strata-X cartridges (30 μm, Phenomenex, Torrance, CA) that were activated with 3 mL of MeOH and preconditioned with 1 mL of H_2O. The hydrolysates were loaded on the cartridges and washed sequentially with 1 mL of H_2O and 1 mL of 5% MeOH in H_2O, and the analytes were eluted with 1 mL of 100% MeOH and 1 mL of MeOH containing 2% formic acid, and both fractions were evaporated to dryness and reconstituted in 2% MeOH in H_2O (LC-MS grade, Fluka) to a final volume of 20 μL prior to MS analysis.

Adductomic DDA-CNL/MS^3 method and data analysis

LC conditions

An aliquot of 1 μL of DNA hydrolysate was injected in a nanoflow Ultra Performance Liquid Chromatography (UPLC) system (Ultimate 3000 RSLCnano UPLC, Thermo Scientific, Waltham, MA). The UPLC system was equipped with a 5-μL autosampler injection loop. Chromatographic separation was achieved using a hand-packed commercially available fused-silica emitter (230 × 0.075-mm ID, 15-μm orifice, New Objective, Woburn MA) with C18 stationary phase (5 μm, 100, Luna Phenomenex, Torrance, CA). The mobile phase consisted of (A) 0.05% (v/v) formic acid in H_2O and (B) CH_3CN. The eluent was held at 2% B for 2 min, brought to 20% B in 24 min, then to 60% B in 10 min, to 98% B in 1 min, and then maintained at 98% for 4 min. The column was re-equilibrated for 4 min. The injection valve position was switched at 6 min to take the injection loop out of the flow path.

MS

All the MS-based analyses were conducted using a hybrid high-field Orbitrap mass spectrometer (Fusion, Thermo Scientific, Waltham, MA). The LC system was interfaced to the mass spectrometer using a Nanoflex ESI ion source (Nanoflex Thermo Scientific, Waltham, MA), which operated in positive ion mode at 2.5 kV. The ion transfer tube temperature was 300°C, and the radio frequency (RF) lens (%) setting was 60. The DDA-CNL/MS^3 method consisted of a full scan with data-dependent MS^2 and a neutral loss MS^3 acquisition (NL-MS^3). The full scan (*m/z* 150–750) was performed with quadrupole filtering, maximum injection time of 50-ms, automatic gain control target of 50%, and a resolution setting of 120,000. Data-dependent MS^2 parameters were dynamic exclusion of 30 s, mass tolerance of ±5 ppm, repeat count of 1, minimum intensity of 2 × 10^4, and a cycle time of 3 s. An MS^2 exclusion list of 18 masses, consisting of unmodified deoxyribonucleosides and their electrostatically bound dimer ions, was included in the method with a mass tolerance of ±5 ppm.[29] The MS^2 scan events were triggered on the basis of an intensity threshold of 5 × 10^3. The MS^2 fragmentation was performed with a quadrupole isolation width of *m/z* 1.5, higher-energy C-trap dissociation (HCD) collision energy 30%, automatic gain control (AGC) value of 400%, maximum injection time of 54 ms, and Orbitrap detection at a resolution setting of 30,000. For the NL-MS^3 data acquisitions, the MS^2 product ions were isolated by the ion trap with an isolation window of *m/z* 2.0, and the MS^3 fragmentation was triggered upon observation of the neutral loss of the 2′-deoxyribose (dR)

or the base moieties (-dR, 116.0474; -G, 151.0494; -A, 135.0545; -T, 126.0429; -C, 111.0433; all within a mass tolerance of ±5 ppm). Masses of the respective ^{15}N-nucleosides were also included. The MS parameters for the NL-MS^3 scan were 30% HCD fragmentation, Orbitrap detection resolution of 15,000, AGC value of 200%, and a maximum injection time of 200 ms.

Data analysis

For DNA adduct screening data analysis, RawConverter (http://fields.scripps.edu/rawconv/) was used to convert the Thermo Scientific raw data files to mzXML files, which were imported into an SQL database, where data filtration on the basis of MS^3 triggering ion *m/z* and retention time was performed. MS^3 triggering ions present in the exposed samples with both *m/z* (±5 ppm) and retention times (±30 s) different from those in the control samples were selected and reported as putative BU-DNA adducts. The absence of the putative BU-DNA adducts in the control samples was further confirmed by generating EICs for all the putative DNA adduct precursor masses at 5 ppm mass tolerance using the Qualbrowser component of the Xcalibur 3.0 software package (Thermo Scientific, Waltham, MA). The MS^2 and MS^3 spectra of each putative DNA adduct were subsequently evaluated for structural information, and the peak areas of the precursor mass were determined.

The presence of the resulting adducts was further confirmed using ^{14}N- and ^{15}N-DNA exposed to the drug, processed as described above, and mixed in a 1:1 ratio prior to LC-MS analysis (Figure S2). In this resulting sample, the presence of co-eluting peaks and MS^3 events corresponding to ^{14}N- and ^{15}N-labeled version of the same adduct supports adduct identification. Briefly, the mass difference between ^{14}N and ^{15}N corresponding to the presence of two, three, four, five, six, seven, eight, nine, or 10 ^{15}N in the molecule was added to each DNA adduct uniquely found in the exposed CT-DNA sample. The resulting masses were manually searched in QualBrowser in the ^{15}N-DNA sample, and MS^2 and MS^3 spectra were investigated and compared with that of the corresponding putative adducts found in CT-DNA. The same retention time (±0.1 min), neutral loss, and fragmentation patterns were expected. Furthermore, the presence of a co-eluting peak and MS^3 event corresponding to the ^{14}N version of the putative DNA adduct was verified. DNA adducts uniquely present in the exposed sample and having the corresponding ^{14}N and ^{15}N peaks were annotated.

Targeted MS method for investigating and quantitating BU-DNA adducts in human blood

LC conditions

The DNA hydrolysates were reconstituted in 20 μL of 2% MeOH in H_2O (LC-MS grade, Fluka) and 1 μL was injected with the same UPLC system and column conditions as described in the adductomic DDA-CNL/MS^3 method. The mobile phase consisted of (A) 5 mM NH_4OAc in H_2O and (B) CH_3CN. The elution program included an isocratic step (2% of B for 5.5 min at 0.9 μL/min), followed by a two-step linear gradient of B (3%/min for 19 min and 19%/min for 2 min, both at a flow rate of 0.3 μL/min) and it concluded with a washing isocratic step, performed at 98% of B for 2 min at 0.3 μL/min. At the end of the elution program, the LC system was equilibrated for 3 min at isocratic conditions (2% of B, 0.9 μL/min). The injection valve position was switched at 6 min to take the injection loop out of the flow path.

Mass spectrometry

The targeted DNA adduct analysis was performed using the targeted MS^2 analysis of 15 BU-derived DNA adducts (Table 2), with a quadrupole isolation window width of *m/z* 1.5, maximum injection time of 54 ms, AGC of 1,000%, and resolution setting of 30,000. MS fragmentation was performed using HCD with a stepped collision energy (25%). The fragmentation of the DNA adduct precursor ions $[MH]^+$ results in neutral loss of the dR, G, A, T, or C moiety to produce the corresponding $[MH\text{-}dR]^+$, $[MH\text{-}G]^+$, $[MH\text{-}A]^+$, $[MH\text{-}T]^+$, and $[MH\text{-}C]^+$ product ions whose masses were extracted for detection of the adducts.

BU-derived DNA adduct quantitation

LODs for adducts *N*7G-Bu-*N*7G (**6**, Figure 1) and *N*7G-Bu-OH (**7**) were determined using their H_2O solutions. LOQ, accuracy, and precision for the MS quantitation method were determined by analyzing CT-DNA enriched with different amounts of synthesized standards **6** and **7** (0, 5, 10, 50, 100, and 200 fmol for adduct **6** and a constant amount of 10 fmol of [$^{15}N_5$]**6**; 0, 1, 5, 10, 30, and 100 fmol for adduct **7** and a constant amount of 5 fmol of [$^{15}N_5$]**7**). Each sample was prepared in triplicate. The LOQ was defined as the lowest amount added to CT-DNA that produced a CV lower than 20%. Accuracy was determined by comparing added and measured amounts of the adducts at each level. Precision was determined by the intraday CV in the triplicate samples. Quantitation of the adducts was done comparing the sample peak area with a calibration curve (0.05, 0.1, 0.3, 0.5, 1, 3, 10, 100, and 200 fmol for adducts **6** and **7**).

DATA AVAILABILITY

The data that support the findings of this study are available from the authors on reasonable request; see author contributions for specific datasets.

SUPPLEMENTAL INFORMATION

Supplemental information can be found online at https://doi.org/10.1016/j.omto.2023.01.005.

ACKNOWLEDGMENTS

MS was carried out in the Analytical Biochemistry Shared Resource of the Masonic Cancer Center, University of Minnesota, supported in part by Cancer Center Support Grant CA-077598. Salary support for P.W.V., head of the Analytical Biochemistry Shared Resource, was provided by the National Cancer Institute Grant CA-211256. The authors would like to thank Dr. Laura Maertens and Carsten Spry for their help with initiating and coordinating the sample collection for this study. We also wish to thank the patients for their participation in this study. Additionally, we acknowledge the hard work and dedication of the nurses and other medical personnel of the M Health

Fairview University of Minnesota Medical Center for their help with collecting the samples. We thank Robert Carlson for editorial assistance.

AUTHOR CONTRIBUTIONS

V.G., S.B., and Y.L. conceived the idea of this manuscript and designed the experiments. Y.L. and V.G. performed the synthesis and characterization of adducts. V.G. and F.J. collected samples from clinics and isolated DNA from blood. V.G., Y.L., and F.J. performed standard purification. V.G. and F.J. performed DNA sample preparation, HRMS, and data analysis. M.L.M. supported sample collection in the clinic together with providing inputs on the project and a clinical point of view. P.W.V. contributed to the optimization of LC-MS-based methods in addition to useful inputs on the project. S.B. and S.S.H. supervised the project. V.G. and Y.L. drafted the manuscript. All authors have read and agreed to the published version of the manuscript.

DECLARATION OF INTERESTS

The authors declare no competing interests.

REFERENCES

1. Diethelm-Varela, B., Ai, Y., Liang, D., and Xue, F. (2019). Nitrogen mustards as anticancer chemotherapies: historic perspective, current developments and future trends. Curr. Top. Med. Chem. *19*, 691–712. https://doi.org/10.2174/1568026619666190401100519.

2. Goodman, L.S., and Wintrobe, M.M. (1946). Nitrogen mustard therapy; use of methyl-bis (beta-chloroethyl) amine hydrochloride and tris (beta-chloroethyl) amine hydrochloride for Hodgkin's disease, lymphosarcoma, leukemia and certain allied and miscellaneous disorders. J. Am. Med. Assoc. *132*, 126–132. https://doi.org/10.1001/jama.1946.02870380008004.

3. Malayappan, B., Johnson, L., Nie, B., Panchal, D., Matter, B., Jacobson, P., and Tretyakova, N. (2010). Quantitative high-performance liquid chromatography-electrospray ionization tandem mass spectrometry analysis of bis-N7-guanine DNA-DNA cross-links in white blood cells of cancer patients receiving cyclophosphamide therapy. Anal. Chem. *82*, 3650–3658. https://doi.org/10.1021/ac902923s.

4. Johnson, L.A., Malayappan, B., Tretyakova, N., Campbell, C., MacMillan, M.L., Wagner, J.E., and Jacobson, P.A. (2012). Formation of cyclophosphamide specific DNA adducts in hematological diseases. Pediatr. Blood Cancer *58*, 708–714. https://doi.org/10.1002/pbc.23254.

5. Stornetta, A., Zimmermann, M., Cimino, G.D., Henderson, P.T., and Sturla, S.J. (2017). DNA adducts from anticancer drugs as candidate predictive markers for precision medicine. Chem. Res. Toxicol. *30*, 388–409. https://doi.org/10.1021/acs.chemrestox.6b00380.

6. Wang, S.S., Zimmermann, M., Zhang, H., Lin, T.Y., Malfatti, M., Haack, K., Turteltaub, K.W., Cimino, G.D., de Vere White, R., Pan, C.X., and Henderson, P.T. (2017). A diagnostic microdosing approach to investigate platinum sensitivity in non-small cell lung cancer. Int. J. Cancer *141*, 604–613. https://doi.org/10.1002/ijc.30747.

7. Wang, L.E., Yin, M., Dong, Q., Stewart, D.J., Merriman, K.W., Amos, C.I., Spitz, M.R., and Wei, Q. (2011). DNA repair capacity in peripheral lymphocytes predicts survival of patients with non-small-cell lung cancer treated with first-line platinum-based chemotherapy. J. Clin. Oncol. *29*, 4121–4128.

8. Zimmermann, M., Wang, S.S., Zhang, H., Lin, T.Y., Malfatti, M., Haack, K., Ognibene, T., Yang, H., Airhart, S., Turteltaub, K.W., et al. (2017). Microdose-induced drug-DNA adducts as biomarkers of chemotherapy resistance in humans and mice. Mol. Cancer Ther. *16*, 376–387. https://doi.org/10.1158/1535-7163.MCT-16-0381.

9. Balbo, S., Hecht, S.S., Upadhyaya, P., and Villalta, P.W. (2014). Application of a high-resolution mass-spectrometry-based DNA adductomics approach for identification of DNA adducts in complex mixtures. Anal. Chem. *86*, 1744–1752.

10. U.S. Food and Drug Administration (2003). Prescribing information of Myleran (busulfan) 2-mg scored tablets. https://www.accessdata.fda.gov/drugsatfda_docs/label/2003/09386slr023_myleran_lbl.pdf.

11. Ciurea, S.O., and Andersson, B.S. (2009). Busulfan in hematopoietic stem cell transplantation. Biol. Blood Marrow Transpl. *15*, 523–536. https://doi.org/10.1016/j.bbmt.2008.12.489.

12. McCune, J.S., and Holmberg, L.A. (2009). Busulfan in hematopoietic stem cell transplant setting. Expert Opin. Drug Metab. Toxicol. *5*, 957–969. https://doi.org/10.1517/17425250903107764.

13. Clift, R.A., Buckner, C.D., Thomas, E.D., Bensinger, W.I., Bowden, R., Bryant, E., Deeg, H.J., Doney, K.C., Fisher, L.D., Hansen, J.A., et al. (1994). Marrow transplantation for chronic myeloid leukemia: a randomized study comparing cyclophosphamide and total body irradiation with busulfan and cyclophosphamide. Blood *84*, 2036–2043.

14. Clift, R.A., Radich, J., Appelbaum, F.R., Martin, P., Flowers, M.E., Deeg, H.J., Storb, R., and Thomas, E.D. (1999). Long-term follow-up of a randomized study comparing cyclophosphamide and total body irradiation with busulfan and cyclophosphamide for patients receiving allogenic marrow transplants during chronic phase of chronic myeloid leukemia. Blood *94*, 3960–3962.

15. Vassal, G., Deroussent, A., Hartmann, O., Challine, D., Benhamou, E., Valteau-Couanet, D., Brugières, L., Kalifa, C., Gouyette, A., and Lemerle, J. (1990). Dose-dependent neurotoxicity of high-dose busulfan in children: a clinical and pharmacological study. Cancer Res. *50*, 6203–6207.

16. McDonald, G.B., Sandmaier, B.M., Mielcarek, M., Sorror, M., Pergam, S.A., Cheng, G.S., Hingorani, S., Boeckh, M., Flowers, M.D., Lee, S.J., et al. (2020). Survival, nonrelapse mortality, and relapse-related mortality after allogeneic hematopoietic cell transplantation: comparing 2003-2007 versus 2013-2017 cohorts. Ann. Intern. Med. *172*, 229–239. https://doi.org/10.7326/M19-2936.

17. Eberly, A.L., Anderson, G.D., Bubalo, J.S., and McCune, J.S. (2008). Optimal prevention of seizures induced by high-dose busulfan. Pharmacotherapy *28*, 1502–1510. https://doi.org/10.1592/phco.28.12.1502.

18. Slattery, J.T., Sanders, J.E., Buckner, C.D., Schaffer, R.L., Lambert, K.W., Langer, F.P., Anasetti, C., Bensinger, W.I., Fisher, L.D., Appelbaum, F.R., et al. (1995). Graft-rejection and toxicity following bone marrow transplantation in relation to busulfan pharmacokinetics. Bone Marrow Transpl. *16*, 31–42.

19. Slattery, J.T., Clift, R.A., Buckner, C.D., Radich, J., Storer, B., Bensinger, W.I., Soll, E., Anasetti, C., Bowden, R., Bryant, E., et al. (1997). Marrow transplantation for chronic myeloid leukemia: the influence of plasma busulfan levels on the outcome of transplantation. Blood *89*, 3055–3060.

20. Palmer, J., McCune, J.S., Perales, M.A., Marks, D., Bubalo, J., Mohty, M., Wingard, J.R., Paci, A., Hassan, M., Bredeson, C., et al. (2016). Personalizing busulfan-based conditioning: considerations from the American society for blood and marrow transplantation practice guidelines committee. Biol. Blood Marrow Transpl. *22*, 1915–1925. https://doi.org/10.1016/j.bbmt.2016.07.013.

21. Andersson, B.S., Thall, P.F., Madden, T., Couriel, D., Wang, X., Tran, H.T., Anderlini, P., de Lima, M., Gajewski, J., and Champlin, R.E. (2002). Busulfan systemic exposure relative to regimen-related toxicity and acute graft-versus-host disease: defining a therapeutic window for i.v. BuCy2 in chronic myelogenous leukemia. Biol. Blood Marrow Transpl. *8*, 477–485. https://doi.org/10.1053/bbmt.2002.v8.pm12374452.

22. Schuler, U., Schroer, S., Kühnle, A., Blanz, J., Mewes, K., Kumbier, I., Proksch, B., Zeller, K.P., and Ehninger, G. (1994). Busulfan pharmacokinetics in bone marrow transplant patients: is drug monitoring warranted? Bone Marrow Transpl. *14*, 759–765.

23. Bartelink, I.H., Lalmohamed, A., van Reij, E.M.L., Dvorak, C.C., Savic, R.M., Zwaveling, J., Bredius, R.G.M., Egberts, A.C.G., Bierings, M., Kletzel, M., et al. (2016). Association of busulfan exposure with survival and toxicity after haemopoietic cell transplantation in children and young adults: a multicentre, retrospective cohort analysis. Lancet Haematol. *3*, e526–e536. https://doi.org/10.1016/s2352-3026(16)30114-4.

24. Myers, A.L., Kawedia, J.D., Champlin, R.E., Kramer, M.A., Nieto, Y., Ghose, R., and Andersson, B.S. (2017). Clarifying busulfan metabolism and drug interactions to support new therapeutic drug monitoring strategies: a comprehensive review. Expert Opin. Drug Metab. Toxicol. *13*, 901–923. https://doi.org/10.1080/17425255.2017.1360277.

25. Iwamoto, T., Hiraku, Y., Oikawa, S., Mizutani, H., Kojima, M., and Kawanishi, S. (2004). DNA intrastrand cross-link at the 5'-GA-3' sequence formed by busulfan and its role in the cytotoxic effect. Cancer Sci. *95*, 454–458. https://doi.org/10.1111/j.1349-7006.2004.tb03231.x.

26. Guidolin, V., Carlson, E.S., Carrà, A., Villalta, P.W., Maertens, L.A., Hecht, S.S., and Balbo, S. (2021). Identification of new markers of alcohol-derived DNA damage in humans. Biomolecules *11*, 366. https://doi.org/10.3390/biom11030366.

27. Stornetta, A., Villalta, P.W., Hecht, S.S., Sturla, S.J., and Balbo, S. (2015). Screening for DNA alkylation mono and cross-linked adducts with a comprehensive LC-MS^3 adductomic approach. Anal. Chem. *87*, 11706–11713. https://doi.org/10.1021/acs.analchem.5b02759.

28. Carrà, A., Guidolin, V., Dator, R.P., Upadhyaya, P., Kassie, F., Villalta, P.W., and Balbo, S. (2019). Targeted high resolution LC/MS^3 adductomics method for the characterization of endogenous DNA damage. Front. Chem. *7*, 658. https://doi.org/10.3389/fchem.2019.00658.

29. Alexander, E.M., Kreitler, D.F., Guidolin, V., Hurben, A.K., Drake, E., Villalta, P.W., Balbo, S., Gulick, A.M., and Aldrich, C.C. (2020). Biosynthesis, mechanism of action, and inhibition of the enterotoxin tilimycin produced by the opportunistic pathogen *Klebsiella oxytoca*. ACS Infect. Dis. *6*, 1976–1997. https://doi.org/10.1021/acsinfecdis.0c00326.

30. Hassan, M., and Ehrsson, H. (1987). Urinary metabolites of busulfan in the rat. Drug Metab. Dispos. *15*, 399–402.

31. Hassan, M., Oberg, G., Ehrsson, H., Ehrnebo, M., Wallin, I., Smedmyr, B., Tötterman, T., Eksborg, S., and Simonsson, B. (1989). Pharmacokinetic and metabolic studies of high-dose busulphan in adults. Eur. J. Clin. Pharmacol. *36*, 525–530. https://doi.org/10.1007/BF00558081.

32. Bouligand, J., Deroussent, A., Simonnard, N., Opolon, P., Morizet, J., Connault, E., Daudigeos, E., Re, M., Paci, A., and Vassal, G. (2007). Induction of glutathione synthesis explains pharmacodynamics of high-dose busulfan in mice and highlights putative mechanisms of drug interaction. Drug Metab. Dispos. *35*, 306–314. https://doi.org/10.1124/dmd.106.012880.

33. Scian, M., and Atkins, W.M. (2015). The busulfan metabolite EdAG irreversibly glutathionylates glutaredoxins. Arch. Biochem. Biophys. *583*, 96–104. https://doi.org/10.1016/j.abb.2015.08.005.

34. Scian, M., and Atkins, W.M. (2015). Supporting data for characterization of the busulfan metabolite EdAG and the Glutaredoxins that it adducts. Data Brief *5*, 161–170. https://doi.org/10.1016/j.dib.2015.09.002.

35. Scian, M., Guttman, M., Bouldin, S.D., Outten, C.E., and Atkins, W.M. (2016). The myeloablative drug busulfan converts cysteine to dehydroalanine and lanthionine in redoxins. Biochemistry *55*, 4720–4730. https://doi.org/10.1021/acs.biochem.6b00622.

36. Souliotis, V.L., Dimopoulos, M.A., and Sfikakis, P.P. (2003). Gene-specific formation and repair of DNA monoadducts and interstrand cross-links after therapeutic exposure to nitrogen mustards. Clin. Cancer Res. *9*, 4465–4474.

37. Stornetta, A., Villalta, P.W., Gossner, F., Wilson, W.R., Balbo, S., and Sturla, S.J. (2017). DNA adduct profiles predict *in vitro* cell viability after treatment with the experimental anticancer prodrug PR104A. Chem. Res. Toxicol. *30*, 830–839. https://doi.org/10.1021/acs.chemrestox.6b00412.

38. Gruppi, F., Hejazi, L., Christov, P.P., Krishnamachari, S., Turesky, R.J., and Rizzo, C.J. (2015). Characterization of nitrogen mustard formamidopyrimidine adduct formation of bis(2-chloroethyl)ethylamine with calf thymus DNA and a human mammary cancer cell line. Chem. Res. Toxicol. *28*, 1850–1860. https://doi.org/10.1021/acs.chemrestox.5b00297.

39. Hemminki, K. (1985). Binding of metabolites of cyclophosphamide to DNA in a rat liver microsomal system and *in vivo* in mice. Cancer Res. *45*, 4237–4243.

40. Palom, Y., Suresh Kumar, G., Tang, L.Q., Paz, M.M., Musser, S.M., Rockwell, S., and Tomasz, M. (2002). Relative toxicities of DNA cross-links and monoadducts: new insights from studies of decarbamoyl mitomycin C and mitomycin C. Chem. Res. Toxicol. *15*, 1398–1406. https://doi.org/10.1021/tx020044g.

41. Walters, K., Stornetta, A., Jacobs, F., Villalta, P.W., Razzoli, M., Grant, M., Zordoky, B., Bartolomucci, A., Borgatti, A., and Balbo, S. (2021). Identification of new candidate biomarkers to support doxorubicin treatments in canine cancer patients. BMC Vet. Res. *17*, 378. https://doi.org/10.1186/s12917-021-03062-x.

42. Moon, S.Y., Lim, M.K., Hong, S., Jeon, Y., Han, M., Song, S.H., Lim, K.S., Yu, K.S., Jang, I.J., Lee, J.W., et al. (2014). Quantification of human plasma-busulfan concentration by liquid chromatography-tandem mass spectrometry. Ann. Lab. Med. *34*, 7–14. https://doi.org/10.3343/alm.2014.34.1.7.

43. Li, Y., Ma, B., Cao, Q., Balbo, S., Zhao, L., Upadhyaya, P., and Hecht, S.S. (2019). Mass spectrometric quantitation of pyridyloxobutyl DNA phosphate adducts in rats chronically treated with *N*'-nitrosonornicotine. Chem. Res. Toxicol. *32*, 773–783. https://doi.org/10.1021/acs.chemrestox.9b00007.